ACS APPLIED NANO MATERIALS

www.acsanm.org Article

Dextran-Based Oxygen Nanobubbles for Treating Inner Retinal Hypoxia

Muhammad Fayyaz, Musarrat Jabeen, Michael S. Tsipursky, and Joseph Irudayaraj*

Cite This: https://doi.org/10.1021/acsanm.1c00084 Read Online

ACCESS | Metrics & More | Article Recommendations | Supporting Information

ABSTRACT: Central retinal artery occlusion (CRAO) is an obstruction of the retinal artery carrying oxygen to the cells in the inner retinal layers. This lack of oxygen may result in irreversible loss of sight if not treated within 24−36 h. We propose a dextran-based oxygen nanobubble (DONB) platform for intravitreal delivery of oxygen to rescue the inner retina from such ischemic damage. The size distribution of DONBs was 119.6 ± 44.9 nm and the zeta (ζ)-potential was −35.54 ± 10.54 mV. The DONBs were found to be stable in amber vials at 5 ± 3 °C for over 4 months and the formulation was not cytotoxic. The therapeutic efficacy of DONBs was first evaluated in retinal precursor cell lines which showed excellent recovery and then in a hypoxia/reperfusion rat eye model. Oxygen distribution measurements and histology indicated excellent recovery of the ganglion and inner retinal cell layers. Electroretinography exhibited normal retinal function. Our unique approach suggests a promising pathway to treat CRAO, a blinding condition for which no effective treatment exists.

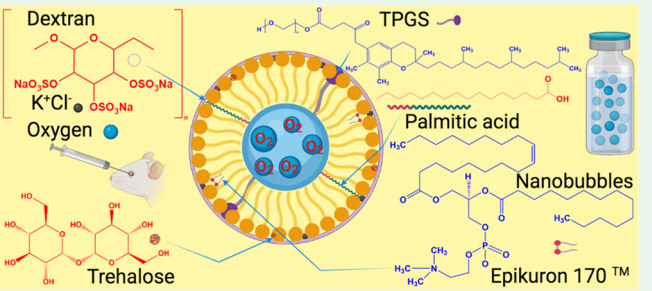

KEYWORDS: *central retinal artery occlusion, ischemia, hypoxia, oxygen nanobubbles, therapeutics*

INTRODUCTION

The central retinal artery occlusion (CRAO) is an ophthalmological emergency and an important cause of acquired irreversible blindness. A consistent and effective treatment for CRAO does not exist at present.[1,2] Occlusion of the central retinal artery from an embolus or a thrombus is similar to the pathophysiology of an ischemic stroke. Anatomically, the central retinal artery is a branch of the ophthalmic artery, and when occluded at the lamina cribrosa level within the optic nerve or the exit of the optic nerve, there is still choroidal circulation that supplies the outer retina with blood flow. Thus, the outer retinal layers are oxygenated, while inner retinal layers are not. Nevertheless, occlusions cause irreversible visual deficit due to the lack of perfusion, which gives rise to a hypoxic state resulting in damage to the inner retinal layers that result in blindness.

After about 72 h, the majority of the CRAOs appear reperfused when examined by fluorescein angiography, and this is sometimes due to the embolus passing or various retinal anastomoses taking over in experimental models; after 4 h, irreversible cell death has been noted, which is progressive and time dependent.[3] However, vision recovery is possible even after delays of 8−24 h with intervention, possibly due to incomplete blockage of the vessel and some diffusion of oxygen from the choroid into outer retinal layers.

It has been shown that inspiration of 100% oxygen can, in the presence of acute central retinal artery obstruction, produce a normal partial pressure of oxygen (pO_2) at the surface of the retina *via* diffusion from the choroid;[4] however, the macula region is much thicker with two ganglion layers and cannot obtain enough oxygen from the choroidal circulation. However, hyperbaric oxygen cannot achieve the therapeutic level of oxygen in the inner retina. Furthermore, access to hyperbaric oxygen treatments is logistically difficult and is not readily accessible to the majority of the patient population. Mitigating the severity of insult due to oxygen deficit, especially during the first few hours is vital, before the onset of permanent damage. Given a lack of current effective treatment options and understanding of the pathophysiology of CRAO, we propose that focused intravitreal oxygen delivery can preserve retinal tissue by mitigating time-dependent ischemic insult to the retinal tissue.

Existing work on perfluorocarbon (PFC)-bearing oxygen nanobubbles yielded a significant improvement in the therapeutic outcome in treating solid tumors'.[5−7] However, clinical trials of (PFC) nanoemulsions eventually failed as a result of various safety issues such as the adverse cerebrovascular effects on cardiopulmonary arrest[8] and PFC-induced microvascular vasoconstriction.[9] Alternatively, cellu-

Received: January 11, 2021
Accepted: June 16, 2021

lose-based oxygen nanobubbles were synthesized in our prior work for cancer treatment but still contain minor amounts of PFC limiting its use in ocular treatment.[10−12] Lipid-coated oxygen microbubbles (LOMs), which serve as ultrasound contrast agents and oxygen carriers, have materialized as promising delivery agents over other drug delivery systems[13−15] because of their high oxygen-loading capability (*i.e.*, >70% v/v).[16] The ultrasound contrast augmentation of LOMs yielded directionality and real-time monitoring for oxygen delivery.[14,17] However, LOMs fail to move through the endothelial gaps (*i.e.*, 400−800 nm) of the vasculature in carcinoma for extravasation due to the large diameter (typically 1 to 2 μm[28]) and have to depend on external stimuli (*e.g.*, ultrasound[18]) to trigger the discharge of oxygen in the vasculature.

Here, we report a unique class of perfluorocarbon-free dextran-based oxygen nanobubble (DONB) formulation. The critical components in the formulation are chosen among the U.S. Food, and Drug Administration (FDA)-approved compounds, which provide a biocompatible environment for incorporating pharmaceutical agents.[19] For formulation optimization, we use rotatable central composite design (RCCD), response surface methodology (RSM), Box−Behnken, and Doehlert designs which are commonly used in the optimization and development of formulations.[20−22] The current formulation of DONBs was tested for oxygen release for ∼2 h to maintain the partial pressure of oxygen within the inner retina high enough to preserve retinal tissue from experimentally induced retinal ischemia. In summary, we have developed a nontoxic, injectable nanobubble formulation that mitigates retinal hypoxia in a rat ocular ischemia/reperfusion model. A scheme of the intravitreal injectable dextran nanobubble formulation for retinal hypoxia is illustrated in Figure 1.

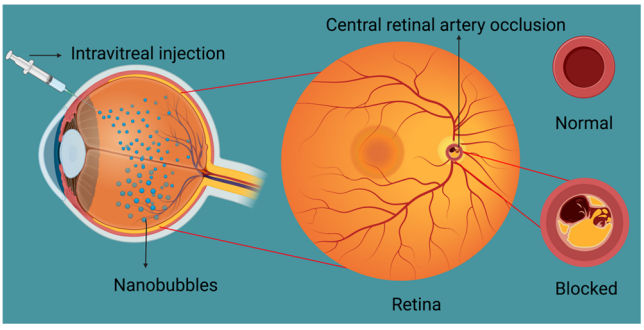

Figure 1. Scheme of intravitreal administration of dextran-encapsulated oxygen nanobubbles for oxygen delivery to retinal cells to treat CRAO, an ischemic disease of the eye. The figure created using BioRender (https://biorender.com/) individual license.

RESULTS AND DISCUSSION

A four-factored rotatable central composite design (RCCD) was used to establish functional relationships among four operating variables: dextran (X_1), potassium chloride (X_2), sonication power (X_3), and pH (X_4) with response variables as average oxygen release (Y_1) at 2 h, the size of oxygen nanobubbles (Y_2), and zeta (ζ) potential (Y_3). After successful optimization with 30 different formulations, we selected the best formulation based on the response set for each variable. Based on the statistical design, the concentration of dextran 0.9% w/v, Epikuron 170 (0.23% w/v), and palmitic acid (0.19% w/v) were used as emulsifiers; potassium chloride was used as an electrolyte to help reduce the size of nanobubbles during sonication and cavitation and to provide additional stability due to ion shielding effect. D-α-Tocopherol poly-(ethylene glycol) 1000 succinate (TPGS) was used to reduce the surface tension and help in the self-assembly of nanobubbles during formulation. Trehalose was used to increase the stability of the dextran core.[23] The excipients used in this work are designated as biocompatible compounds by the U.S. Food and Drug Administration (FDA).[19] The schematic of DONBs encapsulating oxygen is shown in Figure 2a. The process involves the addition of potassium chloride into the sonicated dispersed phase of sterile water for injection at 4 °C. The optimal potassium chloride concentration (0.06% w/v) and sonication power (50 watts) were considered to minimize the nanobubble size. The details of optimization studies are presented in Supplementary Note S1 and Tables S1−S3. The optimization model fitness was established and explained in Supplementary Figure S1 and Note S2. The dextran sulfate sodium 200 kDa is used as the core−shell in the formulation and shows a direct relationship with oxygen release (Supplementary Figure S2, Table S4, and Note S3). The potassium chloride and sonication power control the size of nanobubbles (50−500 nm); the effects of potassium chloride as an electrolyte and sonication power on the size are described in the supplementary section (Supplementary Figure S3, Table S5, and Note S4). A similar pattern of nanobubble size reduction by ultrasonic energy and frequency was investigated by Yasuda et al.[24] The pH of the medium plays a vital role in controlling the ζ-potential of nanobubbles[25] as described in the supplementary section (Supplementary Figure S4, Table S6, and Note S5). In our formulation, by shifting the pH from alkaline to slightly acidic, the ζ-potential shifts toward a negative charge (*i.e.*, negative potential) when there is oxygen inside the shell and nanoparticles are made with reagents that comprise of negative charges.[26] In our formulation, trehalose could contribute to stringency by shielding attractive forces between particles and in preventing aggregation. Negative potential is common when such ingredients are present.[27,28] The ζ-potential measurement illustrates that DONBs are negatively charged with an electrical dual layer, apparently due to the adsorption of negative OH^- ions at the water/gas boundary. The ζ-potential of the final optimized formulation was -35.54 ± 10.54 mV, as presented in Figure 2b. The electrical dual layer that plays a critical role in the creation of stable nanobubbles in aqueous solutions not only provides a repulsive force to avoid nanobubbles aggregation and coalescence but also decreases the surface tension at the water/gas boundary to reduce the internal pressure inside each bubble.[26,29] This mechanism helps to improve the stability of the formulation and decreases toxicity in two ways. First, it increases the colloidal stability; and second, the final formulation can be free from any preservatives owing to its slightly acidic pH, inhibiting microbial growth.[30−32] The biosafety of excipients used in the formulation was evaluated on retinal precursor cells R28 and retinal pigment epithelial cells (ARPE-19); the details are mentioned in Supplementary Figure S5 and Note S6.

Dextran is water-soluble and not efficient in self-assembly; therefore, we used complementary ingredients such as Epikurion 170 and palmitic acid as they assist in the self-assembly process. The size distribution and concentration of

https://doi.org/10.1021/acsanm.1c00084
ACS Appl. Nano Mater. XXXX, XXX, XXX−XXX

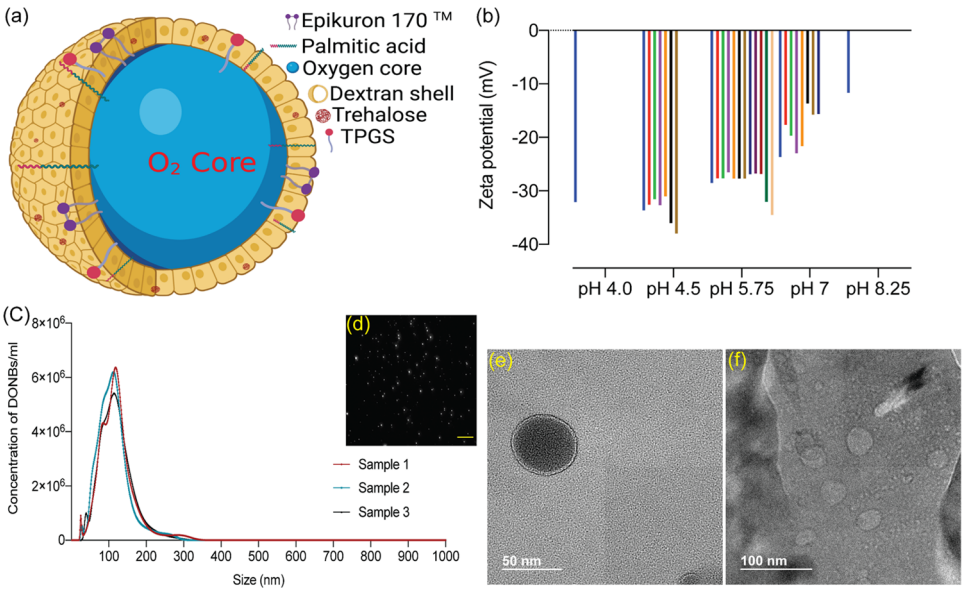

Figure 2. Characterization of DONBs. (a) Schematic of DONBs comprising of dextran shell, encapsulating oxygen. (b) ζ-Potential of DONBs in different pH media. (c) Concentration and size distribution of DONBs/mL and (d) image of floating DONBs obtained by NTA (NanoSight NS300) scale bar = 10 μm. (e, f) Cryo-TEM of DONBs. (a) Created using BioRender (https://biorender.com/) individual license.

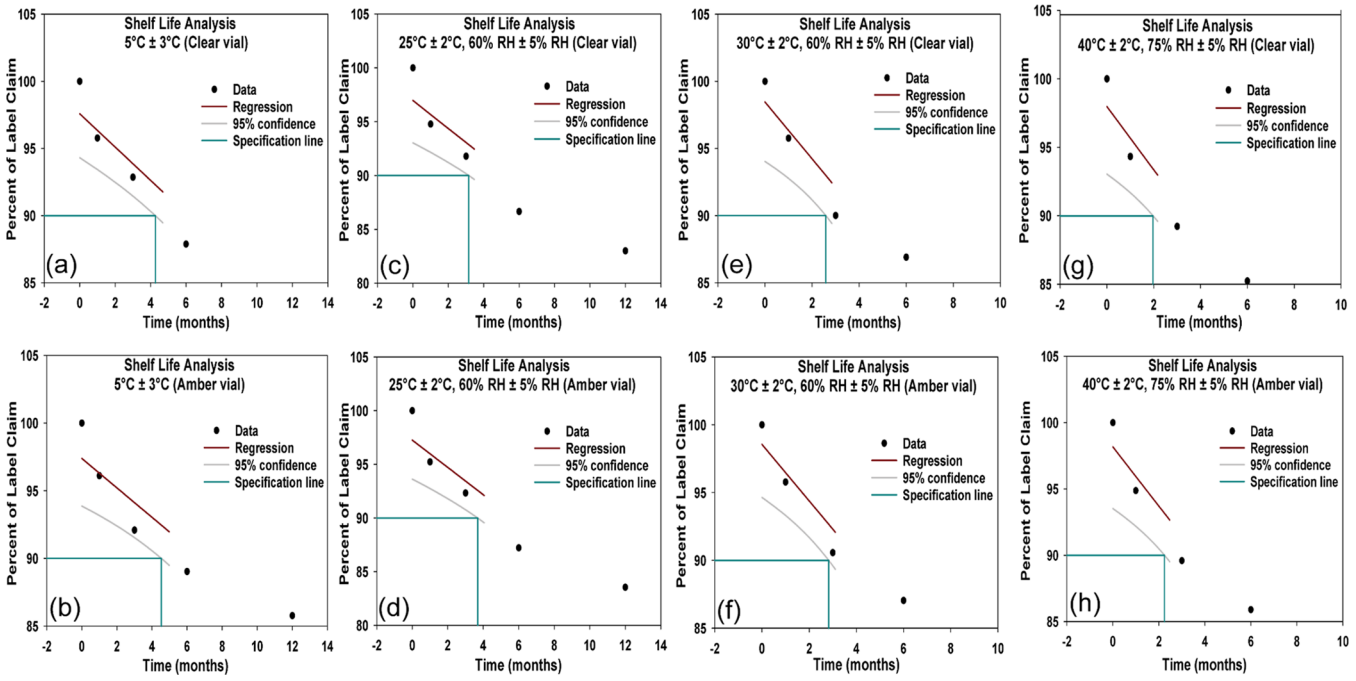

Figure 3. Stability studies of DONBs at different storage conditions and containers. (a, b) Shelf-life at 5 ± 3 °C in clear and amber vials. (c, d) Shelf-life at 25 ± 2 °C in clear and amber vials and 60% relative humidity. (e, f) Shelf-life at 30 ± 2 °C in clear vial and amber vials at 60% relative humidity. (g, h) Shelf-life at 40 ± 2 °C in clear and amber vials at 75% relative humidity.

DONBs/mL were measured using nanoparticle tracking analysis (NTA, NanoSight NS300). The size distribution of the final optimized formulation used in all of the *in vitro* and *in vivo* studies was 119.6 ± 44.9 nm and the concentration of DONBs was 5.26×10^8 nanobubbles/mL (Figure 2c,d). The structure and morphology of nanobubbles were examined by transmission electron microscopy (TEM; JEM-2100F, JEOL, Japan). The TEM image (Figure 2e,f)) shows the core−shell structure and size, in agreement with the size distribution measurement with NTA. The size distribution of nanobubbles plays an important role in tissue and cell uptake.[33,34] This is also addressed with hyperspectral dark-field microscopy (HS-DFM) experiments described in the later sections where the physical uptake of DONBs by cells is addressed.

The optimized formulation was subjected to stability studies per the International Council for Harmonization of Technical Requirements for Pharmaceuticals for Human Use (ICH) and FDA criteria.[35−37] The formed nanobubbles exhibited relatively short- and long-term stability in a liquid state depending upon the storage container and storage conditions (Figure 3). The nanobubbles were placed at room and accelerated temperature and at a different relative humidity (%

https://doi.org/10.1021/acsanm.1c00084
ACS Appl. Nano Mater. XXXX, XXX, XXX−XXX

RH) conditions and the shelf-life evaluated (statistical analysis was performed with the SigmaPlot version 14.0). Our result shows that the shelf-life of DONBs in the amber and clear vial container at 5 ± 3 °C was 4.52 and 4.26 months, respectively, in Figure 3a,b. The shelf-life of nanobubbles in amber and clear vials at 25 ± 2 °C, 60 ± 5% RH was 3.68 and 3.14 months, respectively (Figure 3c,d), whereas that at 30 ± 2 °C, 60 ± 5% RH was 2.96 and 2.82 months, respectively (Figure 3e,f). However, at extreme accelerated temperature and humidity, 40 ± 2 °C, 75 ± 5% RH, the shelf-life reduced to 2.24 and 1.96 months in amber and clear vials, respectively (Figure 3g,h). From the shelf-life analysis studies, we conclude that the ideal storage conditions for our DONB formulation are 5 ± 3 °C in amber-colored vials. Oxygen measurements were consistent per the recommendation by the U.S. FDA and ICH guidelines for the new formulations.[35,36]

The percent oxygen loading in nanobubbles was evaluated using a previously reported method elsewhere[38] by designing a separate set of experiments to assess the effect of dextran concentration on oxygen loading in the DONB formulation as measured in the media in the dissolved form. As shown in Figure 4, the oxygen loading in different formulations

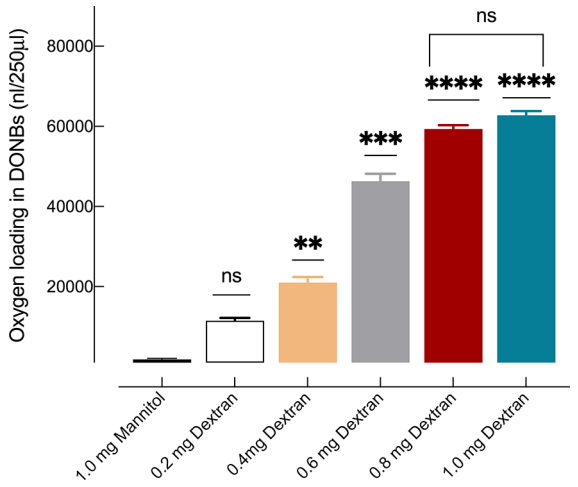

Figure 4. Effect of dextran concentration on oxygen loading in the DONB formulation at a constant oxygen pressure of 2 atm. Dextran concentration of 0.2, 0.4, 0.6, 0.8, and 1.0 mg/mL resulted in the oxygen loading of 11492, 20992, 46316, 59312, and 62760 nL oxygen/250 μL of DONBs, respectively. The oxygen loading in mannitol at 1.0 mg/mL is 1837 nL/250 μL (mean ± standard deviation (SD), n = 3. ****p < 0.00001 *vs* mannitol solution only as control).

synthesized with the same method using the constant oxygen gas pressure of 2 atm but with different concentrations of dextran was measured, with mannitol as control. The oxygen loading was tested as a measure of the displacement of liquid in the microliter syringe, as explained in the methods section. This displacement was measured as 11492, 20992, 46316, 59312, and 62760 nL/250 μL of DONBs synthesized when 0.2, 0.4, 0.6, 0.8, or 1.0 mg of dextran was, respectively, used in the formulation. However, no significant difference in oxygen encapsulation for dextran concentration between 0.8 and 1.0 mg was observed. This finding also supports our optimization studies by the RCCD analysis. By increasing the concentration of dextran, the volume of oxygen loading increased as a direct relationship, indicating that dextran is the critical component of the nanobubble shell.

Epikurion 170 consists of lecithin and phospholipid dispersions, as well as lysolecithin micelles. The micelle formation provides basic information on the mechanism of interaction of zwitterionic phospholipids with dextran sulfate. The addition of dextran sulfate to lecithin dispersions or lysolecithin micelles in the presence of potassium chloride produced insoluble complexes. The formation of the insoluble complex of lecithin or lysolecithin with dextran sulfate represents[39] mutually enhancing interactions involving both positive and negative charges of zwitterionic phospholipids. These are the direct electrostatic interaction between the phospholipid choline nitrogen and the sulfate groups of dextran sulfate and the potassium chloride cross-linking of phosphate groups to the sulfate groups or the phosphate groups of neighboring phospholipids.

The oxygen release profile of DONBs was measured by monitoring the oxygen release rate in artificial (simulated) fluids at 35 °C. The DONBs were added to artificial aqueous humor, vitreous humor,[40,41] and porcine serum at 35 °C in a nitrogen environment, and the dissolved oxygen concentration of the final mixture was measured with a fiber-optic OxyLite Oxford Optronix oxygen probes over time. The oxygen measured is the dissolved oxygen based on our calibration experiments (Figure 5). In all of the three simulated media, after the addition of the DONBs, the dissolved oxygen concentration increased slowly. The highest concentration of oxygen was achieved at 75−90 min in the simulated fluids and then declined because the dissolved oxygen diffused into the nitrogen environment. Notably, the release of oxygen in the aqueous humor not only peaked slightly earlier (Figure 5a) than vitreous humor (Figure 5b) and porcine serum (Figure 5c) but also declined faster; this is because the higher viscosity of vitreous humor and serum helps to sustain the release of oxygen in the vitreous and porcine serum gradually. We used 0.5 mL of simulated aqueous/vitreous and porcine serum as dissolution media and 0.25 mL of DONBs in each set of experiments.

To evaluate *in vitro* hypoxia recovery, we incubated R28 and ARPE-19 cells in the hypoxic chamber, using a mixture of gases (2% O_2, 10% CO_2, and 88% N_2) per manufacturer's protocol to create a hypoxic environment for cell culture (adopted from STEMCELL Technologies).[42] The DONBs were incubated for 6 and 12 h, and cell viability was evaluated by 3-(4,5-dimethylthiazol-2-yl)-2,5-diphenyl tetrazolium bromide (MTT) assay by modifying the established protocol to confirm that nanobubbles are noncytotoxic.[33] The results are shown in Figure 6a for the R28 cell line, which indicates a significantly improved survival in the presence of DONBs, in a hypoxic environment up to 12 h with more significant rescue potential at 12 h. In the same experiment for ARPE-19 cells (Figure 6b), however, the results indicated that cells mostly survived at 6 h and even after 12 h of hypoxia due to the "hardy" nature of the cells. Therefore, there was only marginal improvement in cell survival with the addition of DONBs, which was not statistically significant. *In vitro* studies with R28 cells were helpful to assess the overall performance of our DONBs since these are retinal precursor cells. This information can help predict whether inner retinal cells such as ganglion cells and Müller cells could potentially be rescued by DONBs *in vivo* or in a clinical setting.

https://doi.org/10.1021/acsanm.1c00084
ACS Appl. Nano Mater. XXXX, XXX, XXX−XXX

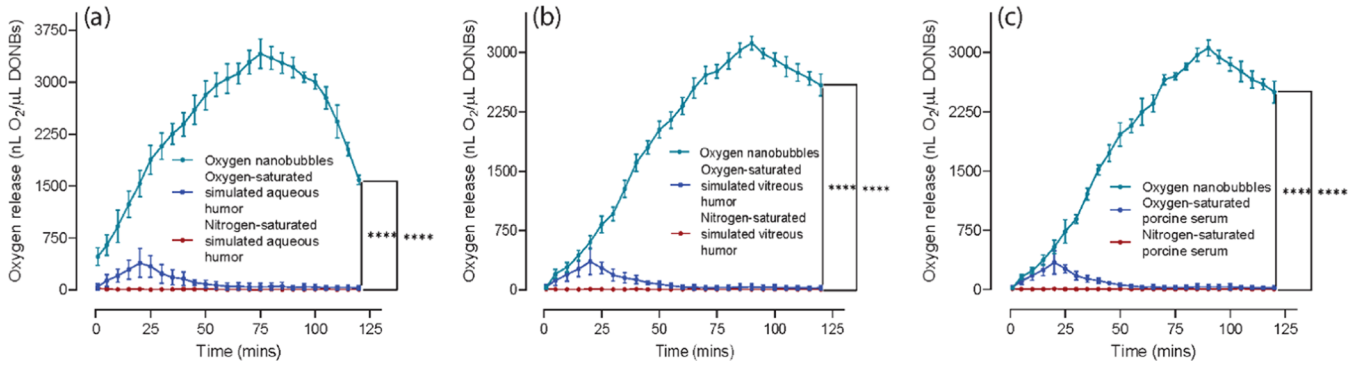

Figure 5. Oxygen release profile of DONBs. (a) Oxygen release profile of DONBs in simulated aqueous humor: oxygen-saturated simulated aqueous humor was used as control. (b) Oxygen release profile of DONBs in the simulated vitreous humor: oxygen-saturated vitreous humor was used as control. (c) Oxygen release profile of DONBs in porcine serum: oxygen-saturated porcine serum was used as control. In all sets of experiments, we used nitrogen-saturated aqueous/vitreous humor and porcine serum as a baseline, and the temperature was maintained at 35 °C (n = 3, p < 0.0001).

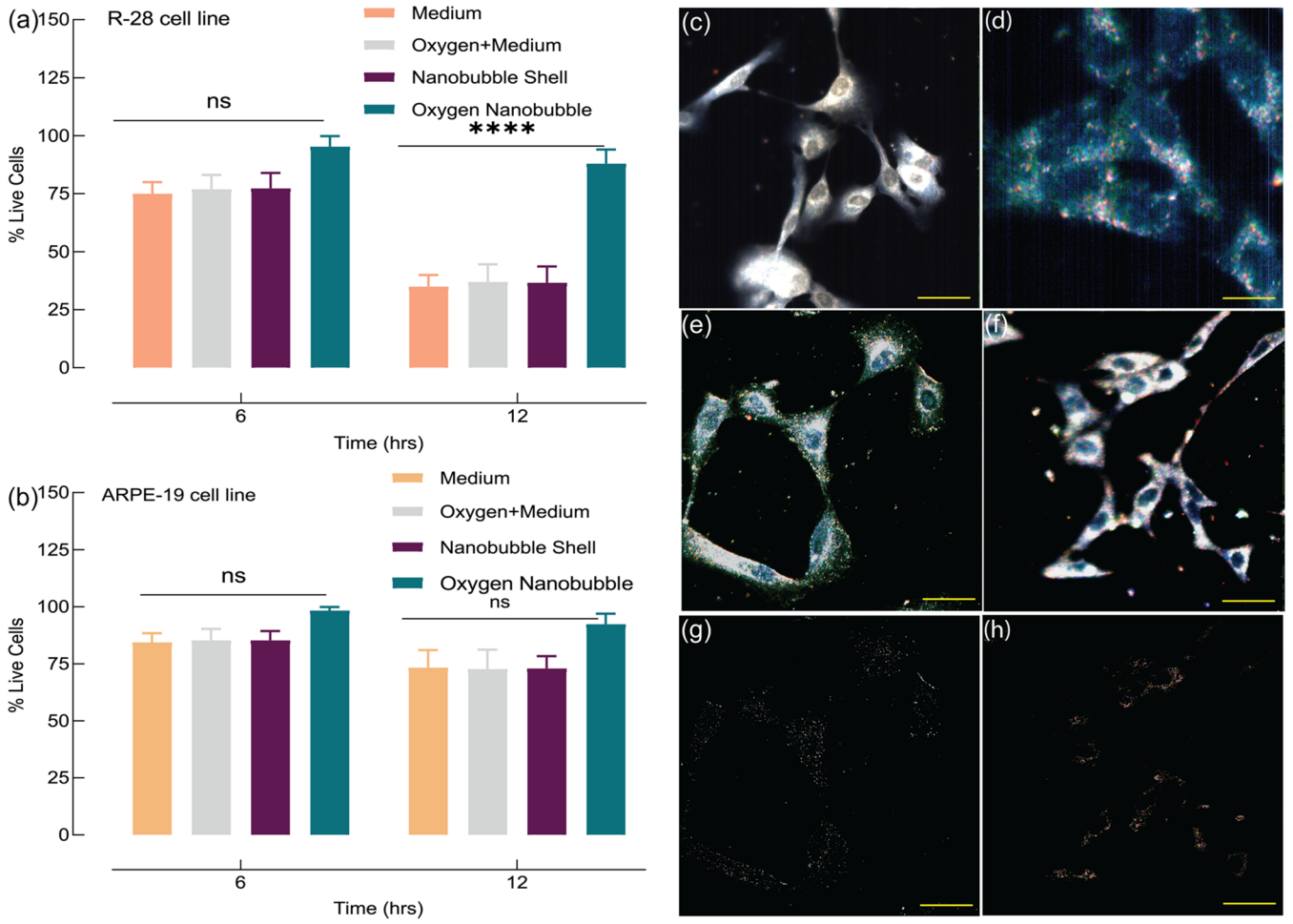

Figure 6. Hypoxia recovery with DONBs in (a) retinal precursor cells (R28) and (b) retinal pigment epithelial cells (ARPE-19). Cells were treated with DONBs along with three controls (culture medium, oxygenated culture medium, and nanobubble shell) and assessed for viability. Results indicate higher viability with DONB treatment (n = 3). (c–h) Cellular uptake of DONBs by hyperspectral dark-field microscopy in R28 and ARPE-19 cells. (c, d) Hyperspectral images of control R28 and ARPE-19 cells. (e, f) R28 and ARPE-19 cells exposed to DONBs, respectively. (g, h) Images after being processed by spectral angular mapping (SAM) algorithm to evaluate the uptake of DONBs by these cell lines, respectively. Scale bar = 15 μm.

The cellular uptake studies by ARPE-19 and R28 cell lines were evaluated with hyperspectral dark-field microscopy (HS-DFM). To identify the DONB intracellularly, a spectral library of DONBs was constructed (Supplementary Figure S6). The spectral library was then used to filter each image using the control image as a blank to identify DONBs in the exposed cell images using ENVI 4.8 software spectral angular mapping (SAM) algorithm. Figure 6c,d shows the respective control.

https://doi.org/10.1021/acsanm.1c00084
ACS Appl. Nano Mater. XXXX, XXX, XXX−XXX

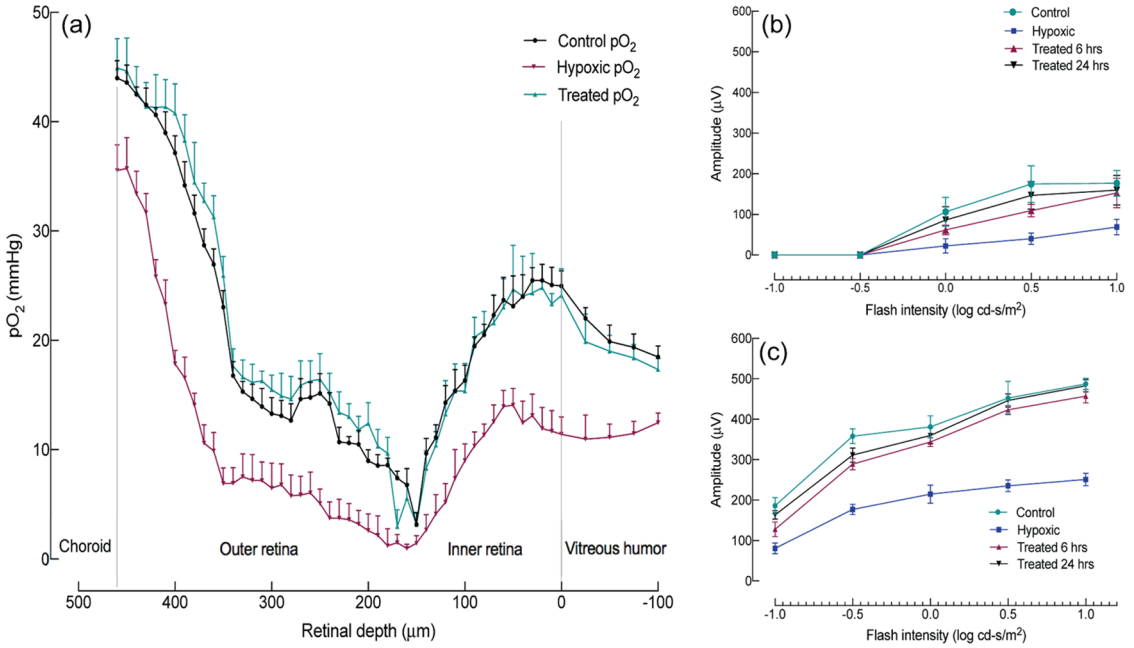

Figure 7. Hypoxia recovery with DONBs. (a) Partial pressure of oxygen (pO_2) measured in control, hypoxic, and treated eyes (n = 6, 3 male and 3 females). Electroretinogram (ERG) studies of a-wave of ERG (b) and b-wave (c) in control, hypoxic, and treated eyes at 6 and 24 h post administration of DONBs.

Figure 6e,f shows the images of R28 and ARPE-19 cells with DONBs. After mapping, the uptake of DONBs by R28 and ARPE-19 cells is shown in Figure 6g,h, respectively. Our results illustrate the uptake of DONBs by R28 and ARPE-19 cells (Figure 6c−h). Our goal is to oxygenate the hypoxic vitreous-retinal environment quickly before permanent damage occurs. If the patient is not treated within 24−36 h after hypoxia, permanent blindness occurs. A key objective of this approach is to rescue the tissues from hypoxia while waiting for the retina to reperfuse to reestablish oxygenation levels from its own blood supply.

After successful viability testing and uptake studies *in vitro*, as the next step *in vivo* experiments were performed. For *in vivo* studies, we used 12-week-old Sprague−Dawley rats (Charles River Inc., CA) per the University of Illinois at Urbana-Champaign Institutional Animal Care and Use Committee (IACUC) Protocol # 108077 (approved 10/2018). Upon arrival, animals were allowed at least 2 weeks for acclimatization. After the acclimatization period, the intraocular pressure (IOP) in the right and left eye was measured for 7 days until the average of 4−5 consecutive values reached the level with a coefficient of variation less than 5%. The data of IOP is presented in Supplementary Figure S7. All IOP measurements were conducted at the same time of day (10 am−12 pm) by the same observers. The IOP measurements began within 5 min of inducing anesthesia, and the animals were awake within 30 min of the IOP measurement. In our experiments, a total of 24 rats were used, 12 males and 12 females. For hypoxia studies, we used a well-known ocular ischemia/reperfusion model.[43−45] The right eye of the animal was used as the control eye, and the left eye was used as the experimental eye throughout the experiments.

As noted in Supplementary Figure S8, after the intravitreal injection of 5 μL of DONB solution, the IOP increased to only 16 mmHg but returned to normal levels within 6 h. This is consistent with or perhaps better than that reported in the literature.[46−48] The IOP was monitored for up to 24 h postinjection. The largest difference in IOP between both eyes was reached at 1.5 h, 16.00 ± 1.45 *vs* 13.54 ± 1.00 mmHg. The intraocular pressure returns to normal at 6 h (13.64 ± 1.06 *vs* 14.28 ± 1.20 mmHg), indicating that a second dose can be administered, if needed. Further, we assessed whether the hypoxic damage to the retina was mitigated in treated *vs* the untreated ischemic eyes. The oxygen concentration in the vitreous cavity of the study eye was determined and compared with untreated eyes using OxyLite Oxford optronix oxygen probes. The measurements in the experimental eye were performed 6 h after DONB treatment (detailed in Note S9). Figure 7a shows intraretinal pO_2 profiles from control, hypoxic, and treated rat eyes in a total of six rats, three males and three females. There is clear evidence that DONBs-treated hypoxic eye had an almost typical pO_2 profile in vitreous (25−20 mmHg), inner retina (5−20 mmHg), outer retina (15−40 mmHg), and choroid (∼45 mmHg) with values in line with the control eye and consistent with the literature.[49−51] The hypoxic eye had much lower pO_2 values for all tissues.

Admittedly, our ischemic model causes more global ischemia, which is akin to an ophthalmic artery occlusion as opposed to retinal artery occlusion. Furthermore, the area of the retina that most crucially requires oxygenation is ∼22.7% (5 mm diameter of the macula while the entire retinal diameter is 22 mm in the human eye). For the clinical evaluation of CRAO, it is critical that the inner layers of the macula are maintained compared to the entire retinal layers to preserve a majority of the vision. Despite the global ischemia in the proposed model, the DONB technology shows excellent promise in mitigating hypoxia. The oxygen requirement for the rat retina is 2×10^6−3×10^6 nL/100 g, and the human retina requires 10^7 nL/100 g/min.[52] Another study established that the inner retinal oxygen consumption is approximately 1200 nM/h on a weight-adjusted basis.[53] The maximum oxygen release from the synthesized DONBs was 3.68×10^6

https://doi.org/10.1021/acsanm.1c00084
ACS Appl. Nano Mater. XXXX, XXX, XXX−XXX

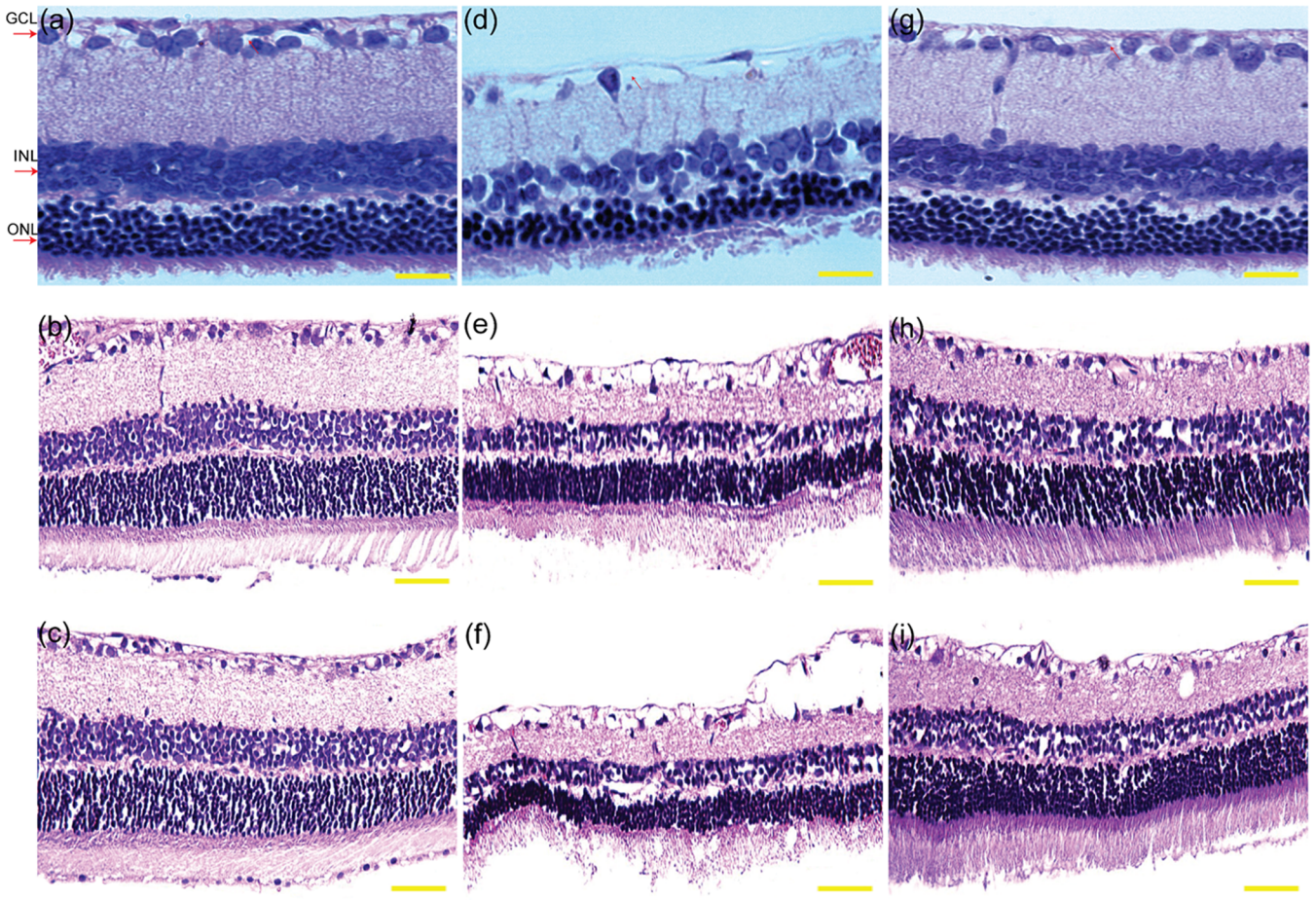

Figure 8. Hematoxylin and eosin (H&E) staining of the enucleated retina to visualize cell damage and retinal layer thickness in control, hypoxic, and treated eyes. In the control retina (panel a−c), all of the layers of retina ganglion cell layer (GCL), inner nuclear layer (INL), and outer nuclear layer are full of cells, and the thickness of the whole retina was intact. The hypoxic retina (panel d−f) shows the most affected cells being the ganglion cells in the upper layer and the overall reduced thickness of the retina. DONBs-treated retina (panel g−i) shows the recovery of ganglion cells from hypoxic insult. The whole thickness of the retina was nearly maintained. Scale bar = 50 μm.

nL/min in simulated aqueous humor, 3.5×10^6 nL/min in the simulated vitreous humor, and 3.35×10^6 nL/min in serum. The recorded data were analyzed according to Henry laws[54] and commercially available online calculator Loligo Systems, Tjele. According to the *in vitro* release study in the simulated aqueous humor, vitreous humor, and serum, DONBs meet the oxygen consumption requirements for the inner retina in rats (5 μL of dose) and humans (50 μL of dose) to rescue from ischemia to revert blindness. In the case of humans, the total retinal oxygen requirement is 10^7 nL/min. The inner retina is approximately 25% of the whole retina, which means 2.5 X 10^6 nL/min is required by the inner retina. The outer retina, including photoreceptors and underlying retinal pigment epithelium, is supplied with oxygen by the choroidal circulation derived from the long and short posterior ciliary arteries and is not infarcted in pure CRAO.[55] Therefore, our main target is the inner retinal recovery in case of hypoxia.

The retinal function was assessed with electroretinogram (ERG) recording of live animals in treated *vs* untreated eyes. The retina is comprised of layers of specialized cells, including photoreceptors (rods and cones) that detect light, and ganglion cells that transmit images to the brain. Specifically, the ERG records electrical signals from the photoreceptors, as well as other cells (Müller cells and bipolar cells) that act as intermediaries between the photoreceptors and the ganglion cells. Here, lower a- and b-wave amplitudes (Figure 7b,c) signify hypoxia impairments in retinal photoreceptor function. In these and other hypoxia endpoints, the nonhypoxic eye serves as a robust negative control for the relative assessment of hypoxia-induced damage. We observed ERG data from six eyes further supporting the claim that DONBs mitigate hypoxic insult. The hypoxic eye clearly shows diminished a- and b-waves, indicative of impaired function. The treated eye at 6 and 24 h had an almost normal response in both a- and b-wave mode, which complies with the control. After each set of experiments, both eyes were enucleated to isolate the retina, used for histological examinations to identify retinal morphological changes according to established protocols[56] for comparison with and without nanobubble treatment. The isolated retina was stained with hematoxylin and eosin (H&E) and used to assess the retinal damage and retinal layer thickness. For each retina, digitized images of control (Figure 8a−c), hypoxic (Figure 8d−f), and treated (Figure 8g−i) were captured and recorded. We observed significant preservation in the DONBs-treated retina in terms of ganglion cell loss, total cell loss, and retinal thickness compared to the hypoxic retina. Our histological study shows the recovery of the retinal layers in the DONBs-treated retina after the ischemic insult in the demonstrated rat model. Further studies are needed to improve the formulation stability, oxygen-loading capacity,

https://doi.org/10.1021/acsanm.1c00084
ACS Appl. Nano Mater. XXXX, XXX, XXX−XXX

disease-specific models, and incorporating larger animals such as rabbit or pig eye models.

CONCLUSIONS

Dextran-based oxygen nanobubbles (DONBs) were synthesized as a carrier for oxygen to reoxygenate the hypoxic retinal tissue, as an emergency treatment for CRAO or related ischemic conditions for the eye. The DONB formulation is stable enough to be stored in a solution form at 4 °C for over 4 months. The nanobubble formulations yielded nanobubbles in the size range from 50 to 500 nm, negative ζ-potential, and good oxygen-loading capacity. *In vitro* and *in vivo* experiments demonstrated that our DONB formulation can help in the successful recovery of intraretinal oxygen levels near-to-normal and rescue the retinal tissue from damage due to hypoxia, confirming oxygen diffusion in the inner retina. Our approach can help in preventing the functional loss of the retina as confirmed with ERG and histological studies, thus preserving vision. We conclude that our DONBs may be a promising approach for the timely delivery of oxygen during a hypoxic insult.

METHODS

Materials. Dextran sulfate sodium salt (200 kDa) (Sigma 67578-5G), D-(+)-trehalose dihydrate (Sigma T5251-10G), potassium chloride (Sigma P9541-500G), D-α-tocopherol poly(ethylene glycol) 1000 succinate (Sigma 57668-5G), and palmitic acid (Sigma P0500) were purchased from Sigma-Aldrich, a subsidiary of Merck KGaA, Merck Millipore Sigma. Epikuron 170 phospholipid deoiled soy lecithin was a kind gift from Cargill, Germany. Sterile water used for injection was USP/EP (RMBIO 10837-184). All chemicals were used as received without any modification. Clear serum vials 7 × 13 mm (cat # 23683) and amber serum vials 7 × 13 mm (cat # 223693) were purchased from Duran Wheaton Kimble Life Sciences (Millville, New Jersey). OxyLite bare fiber-type oxygen sensors product code "NX-BF/O/E" was purchased from Oxford Optronix, Oxford, U.K.

Synthesis of Nanobubbles. The DONBs were synthesized using ultrasonication cavitation and the high-speed homogenization method. Briefly, 50 mL of sterile water for injection (USP) was oxygenated and sonicated, 1 mL (0.06% w/v) of potassium chloride was added to reduce the size of bubbles under continuous oxygenation and sonication at 50 watts/s for 5 min using Branson sonifier SFX250, and the oxygenation level was maintained at a partial pressure >200 mmHg. After 5 min, 3 mL (0.23% w/v) of Epikuron 170 and 2 mL (0.028% w/v) of D-α-tocopherol poly(ethylene glycol) 1000 succinate (TPGS) were added to the solution. The solution was switched to homogenization at 18 000 rpm using Ultra-Turrax T18 homogenizer (IKA, Staufen, Germany). During homogenization, 5 mL (0.9% w/v) of dextran was added, and homogenization speed was increased to 22 000 rpm for 5 min. The resulting solution was sonicated at 50 watts/s for 5 min. Then, 1.5 mL of (0.19% w/v) palmitic acid was added, followed by the addition of 2 mL (0.40% w/v) of trehalose solution. The whole process was performed in an ice bath, and the internal temperature of the solution was maintained at 4 °C. The DONBs were filtered with a 0.22 μm filter and stored in clear and amber-colored borosilicate glass vials for characterization studies.

Size Distribution and Nanobubble Concentration Measurements. Nanoparticle tracking analysis (NTA, NanoSight NS300, Malvern Instrument) was used with a blue laser light source (λ = 488 nm) to measure the hydrodynamic size and concentration of nanobubbles. The NTA was equipped with a 20× magnification microscope and a high-speed camera. When the laser light struck the particle, scattering faculae formed. The scattering faculae were tracked and recorded by the high-speed camera. Each result gathered an average of five measurements, and the movie lasted for 60 s, captured at 25.0 frames/s. The camera level was usually set at 10, the threshold was set at 3, and the solution viscosity was kept at 1 cP.

ζ-Potential Measurements. Electrophoretic mobility and the light scattering method were used for ζ-potential measurement using Zetasizer Nano ZS90 (Malvern, Worcestershire, U.K.). The dispersion technology software version 7.13 was used to record the ζ-potential measurement and analysis. As proposed by ISO13099, the Smoluchowski model was used to calculate the ζ-potential values of nanoparticles in aqueous media. ζ-Potential experiments were averaged from three runs of between 10 and 100 scans at 25 °C.

Stability Studies. The shelf-life of DONB formulations stored in different containers at different temperatures and humidity conditions was assessed per FDA and ICH guidelines.[35−37] The single batch of DONB stability data was analyzed with SigmaPlot version 14 (SYSTAT Software Inc., San Jose, CA). Nanobubbles were placed at 5, 25, 30, and 40 °C with the controlled relative humidity of 60 and 75% in clear and amber-colored vials. After a specified period, the concentration of oxygen was measured and compared with the initial concentration of oxygen when prepared as a control.

Excipients Toxicity Studies Were Conducted with ARPE-19 and R28 Cell Lines. Cell viability was assessed with ARPE-19 and R28 cell lines, in response to treatment with nanobubble excipients, using the [3-(4,5-dimethylthiazol-2-yl)-2, 5-diphenyl tetrazolium bromide] (MTT) assay. The MTT reagent (cat no. M6494, Thermo Fisher Scientific) was prepared by dissolving 5 mg of MTT per 1 mL of phosphate-buffered saline (PBS) (cat no. 21-040-CV, Corning), filter-sterilized using 0.22 μm filter, and stored in dark at 4 °C. The yellow-colored MTT was reduced to purple formazan by the mitochondria of living cells. The cells were grown to 80−90% confluence in a T-25 flask, trypsinized and seeded into a 96-well plate at a density of 10 000 cells/well. The cells were incubated at 37 °C and allowed to adhere for 24 h, then treated for 48 h at 37 °C with various concentrations of excipients (dextran 0.2−1.6% w/v, palmitic acid 0.06−0.24% w/v, Epikuron 170 0.05−0.45% w/v, potassium chloride 0.005−0.08% w/v, TPGS 0.005−0.045% w/v, trehalose 0.05−0.7% w/v). To each well, 20 μL of reagent was added including control wells and incubated for 4 h at 37 °C, followed by the addition of 150 μL of MTT solvent (0.1% acidified IGEPAL CA-630 in isopropanol) to each well, covered with aluminum foil and agitated on an orbital shaker for 15 min. The absorbance was measured at 570 nm; the results are presented as the percentage of the control values for cells grown concurrently in the absence of any excipients.

Measurement of the Amount of Oxygen Gas into Dextran Nanobubbles. The amount of oxygen loading was determined using a previously reported method.[38] Briefly, five different formulations of DONBs were synthesized using 0.2, 0.4, 0.6, 0.8, or 1.0 mg of dextran. For each formulation, 0.25 mL of DONBs was taken in a 3 mL syringe. A two-way Luerlock stopcock was coupled to the syringe and the air was displaced from the syringe and stopcock by depressing the plunger. The stopcock was closed and coupled to a 250 μL syringe without a plunger but containing 30 μL of water. The plunger of the large syringe was withdrawn to generate a vacuum, releasing oxygen from the DONBs. The stopcock was opened, and the plunger was depressed to transfer the released oxygen into the small syringe, where its volume was measured according to the displacement of 30 μL bolus of water.

Cellular Uptake of DONBs. Evaluation of DONBs uptake by R28 and ARPE-19 cell lines was carried out using hyperspectral dark-field microscopy. For imaging, cells were cultured on positively charged slides and allowed to adhere. After 24 h, the medium was replaced with the DONBs and incubated for 2 h at 37 °C. The slides were then washed with phosphate-buffered saline (PBS), and cells were fixed with 4% paraformaldehyde. The method used for the identification and quantification was developed in our prior work and published elsewhere.[11,57] Briefly, the method uses advanced optics and algorithms for the investigation of hyperspectral dark-field images to analyze the interfaces between cells and administered compounds. This nondestructive technique quantitatively tracks the intracellular biodistribution of nanobubbles and allows precise observations of accumulation patterns. The uptake/accumulation of DONBs in intracellular space after 2 h of incubation was adopted following several repetitive experiments. To identify and quantify the DONBs in

https://doi.org/10.1021/acsanm.1c00084
ACS Appl. Nano Mater. XXXX, XXX, XXX−XXX

cells, first, we create the spectral library of DONBs and save them in the spectral library folder. The cells grown on positively charged slides without DONB administration were scanned and captured as a control image. The spectral data were analyzed using the CytoViva software (ENVI 4.8 and ITT Visual Information Solutions). Hyperspectral information is normally assembled (and described) as a data cube with spatial information obtained in the $X-Y$ plane and spectral data described in the Z-direction. The spectral libraries were collected by defining a region of interest (ROI) from the scanned specimen. The ROI choice allows choosing pixels that best describe the morphological state of cells. When the required specific spectral libraries were recognized, they were kept in a spectral library folder by the CytoViva ENVI software for the following spectral mapping of the hyperspectral images of other specimens. Each spectrum involved in the library was collected from a single pixel imaged with a 40× objective. Eventually, a standard spectral angle mapper (SAM) was applied to estimate the resemblance between the pixels of the image and the spectral library pixels saved in the CytoViva ENVI software folder. SAM was performed by measuring the angle between the image and spectral libraries and using them as trajectories in the n-D space, where "n" denotes the number of bands. The best spectral angle match was obtained when the angle between the saved spectral libraries and specimen spectra was the least. After successfully mapping, the DONBs were identified with the SAM algorithm.

Intraocular Pressure Measurement. The intraocular pressure (IOP) of Sprague–Dawley rats' eyes were measured to establish the normal IOP in this animal model after 2 weeks of acclimatization. All measurements were performed between 10:00 am and 12:00 pm to reduce IOP variations due to circadian rhythm for 1 week. All animals weighed between 250 and 300 g; 24 rats were male and 24 were female. Before IOP determinations, one drop of 0.5% proparacaine hydrochloride was administered to each eye. The IOP was measured using a Tono-Pen XL Tonometer (Medtronic). The instrument displays three automated means, and the statistical reliability of the average measurement (SRAM) was <5%. If the SRAM were >5%, another measurement was taken. The mean IOP with standard deviation was estimated to determine the range of normal IOP for our animals.

Preparation for Ocular Ischemia Model in Rats. The hypoxia model was developed according to the previously reported method elsewhere.[43] The experiments were performed on a total of 24 Sprague–Dawley rats, bodyweight 250–300 g. The rats were housed essentially two per cage, with a 12:12 h light/dark cycle. The ambient light level averaged 290 lx, which ensured normal photoreceptor density. The rats were anesthetized with an intraperitoneal injection of ketamine/xylazine/acepromazine, 50:10:1.5 mg/mL cocktail. The dose of the cocktail administered was 0.1 mL/100 g of rat weight. Ketamine was used to maintain the anesthesia, if needed. After anesthesia, the rat was placed under the surgical microscope, focusing on the cornea. Underneath the surgical microscope, forceps was used to softly hold the eye. A 30 gauge needle was gently inserted into the anterior chamber about the center between the zonule fibers and the apex of the cornea with caution to avoid scraping or piercing the iris, lens, or inner corneal surface and to avoid piercing the cornea multiple times or more than once. The needle was inserted into the anterior chamber, and the tubing was secured to limit its movement. The IOP was raised to ∼60 mmHg for 90 min to create ischemia and checked with a Tono-Pen XL Tonometer (Medtronic). Details of the experiment for the ocular ischemia model are provided in the Supporting Information (Note S7). Oxygen measurement *in vivo* is detailed in the Supporting Information, Note S9.

Electrophysiological Setup and Recording. The ERG recording was performed according to the reported method.[58,59] Before performing ERG recording, the animals were dark-adapted overnight, and their supervision was done under dim red light (λ > 600 nm). The setup was placed on an ELpF vibration isolation platform (Kinetic Systems, Boston, MA) for system stability in a vibration-free environment. A custom-built aluminum mesh Faraday cage was used to block the external electromagnetic interference (EMI or noise). The animals were anesthetized and mydriasis was induced bilaterally by applying a topical drop of 1% atropine (tropicamide 1%; Alcon) to both eyes. The custom-built Ganzfeld dome light stimulation device was used. Ganzfeld dome ensures a homogeneous illumination anywhere in the retina, with multiple reflections of the light generated by light-emitting diodes (LED), providing a wide range of light intensities. Visual signals were elicited by light pulsed from LEDs; the frequency of the light pulses was controlled by the analog out channel of the AD board. For high-intensity illuminations, a single LED placed close (1 mm) to the eye was used. The bioamplifier was attached to PowerLab/SP16 using BNC cables, and PowerLab was attached to the computer. Data was attained, digitized, and recorded using a Lab Chart 5.1 software (AD Instruments) that operates on a Dell OptiPlex system Windows XP SP3 32 bits (Dell Inc.). Further details of the ERG procedure is mentioned in the Supporting Note S8.

H&E Staining. After treatment with DONBs, the eyes were enucleated after 12 h (note that the injection volume in rat eye was 5 μL and the nanobubbles used were without dilution), and the retina was separated according to established protocols.[56] To assess retinal damage, the thickness of retinal layers and cell damage was measured on hematoxylin and eosin (H&E)-stained sections. For each section, digitized images of the retina were captured using a digital imaging system Olympus Q-color 5 RTV (5 Megapixel) equipped with Olympus microscope BX51 (Olympus, Tokyo, Japan) at 20× magnification. The camera was operated with Q Capture Pro 7 software (Teledyne digital imaging, Inc., Surrey BC Canada).

■ ASSOCIATED CONTENT

Supporting Information

The Supporting Information is available free of charge at https://pubs.acs.org/doi/10.1021/acsanm.1c00084.

Dextran-based oxygen nanobubble optimization and associated experiments related to animal data (PDF)

■ AUTHOR INFORMATION

Corresponding Author

Joseph Irudayaraj − *Department of Bioengineering and Nick Holonyak Micro and Nanotechnology Laboratory, University of Illinois at Urbana-Champaign, Urbana, Illinois 61801, United States; Biomedical Research Centre (BRC), Mills Breast Cancer Institute, Carle Foundation Hospital, Urbana, Illinois 61801, United States; Cancer Centre at Illinois (CCIL), University of Illinois at Urbana-Champaign, Urbana, Illinois 61801, United States; Carl R. Woese Institute of Genomic Biology, University of Illinois, Urbana-Champaign, Illinois 61801, United States; Carle-Illinois College of Medicine, Champaign, Illinois 61820, United States;* orcid.org/0000-0002-0630-1520; Phone: 217-300-0525; Email: jirudaya@illinois.edu

Authors

Muhammad Fayyaz − *Department of Bioengineering, University of Illinois at Urbana-Champaign, Urbana, Illinois 61801, United States; Biomedical Research Centre (BRC), Mills Breast Cancer Institute, Carle Foundation Hospital, Urbana, Illinois 61801, United States*

Musarrat Jabeen − *Department of Bioengineering, University of Illinois at Urbana-Champaign, Urbana, Illinois 61801, United States; Biomedical Research Centre (BRC), Mills Breast Cancer Institute, Carle Foundation Hospital, Urbana, Illinois 61801, United States;* orcid.org/0000-0003-1668-6548

Michael S. Tsipursky − *Vitreo-Retinal Surgery, Ophthalmology Department, Carle Foundation Hospital, Champaign, Illinois 61802, United States; Carle-Illinois*

https://doi.org/10.1021/acsanm.1c00084
ACS Appl. Nano Mater. XXXX, XXX, XXX−XXX

College of Medicine, Champaign, Illinois 61820, United States; orcid.org/0000-0002-7693-4294

Complete contact information is available at: https://pubs.acs.org/10.1021/acsanm.1c00084

Author Contributions

J.I. conceived the idea and provided resources and overall supervision; M.F. designed, performed the experiments, and wrote the manuscript. M.J. performed cell studies and assisted and performed animal studies. M.S.T. provided guidance on eye studies, clinical relevance, and manuscript writing. All authors discussed the results. J.I. and M.S.T. reviewed and edited the manuscript.

Notes

The authors declare the following competing financial interest(s): We have filed a provisional patent application on the technology through the OTM at UIUC.

■ ACKNOWLEDGMENTS

J.I. is supported by the University of Illinois at Urbana-Champaign startup grants. The authors are thankful for Epikuron 170 as a gift from Cargill Inc. Germany. The support and help for animal studies from the Beckman Institute for Advanced Science and Technology are much appreciated. The authors are thankful to the staff members and facilities for the Cryo-TEM imaging at Material Research Laboratory at the University of Illinois at Urbana-Champaign, United States. All authors agree that there is no conflict of interest.

■ REFERENCES

(1) Fraser, S. G.; Adams, W. Interventions for acute non-arteritic central retinal artery occlusion. *Cochrane Database Syst. Rev.* **2009**, *2009*, No. CD001989.

(2) Flaxel, C. J.; Adelman, R. A.; Bailey, S. T.; Fawzi, A.; Lim, J. I.; Vemulakonda, G. A.; Ying, G.-s. Retinal and ophthalmic artery occlusions Preferred Practice Pattern. *Ophthalmology* **2020**, *127*, P259−P287.

(3) Arjamaa, O.; Nikinmaa, M. Oxygen-dependent diseases in the retina: Role of hypoxia-inducible factors. *Exp. Eye Res.* **2006**, *83*, 473−483.

(4) Hayreh, S. S.; Zimmerman, M. B.; Kimura, A.; Sanon, A. Central retinal artery occlusion.: Retinal survival time. *Exp. Eye Res.* **2004**, *78*, 723−736.

(5) Prato, M.; Magnetto, C.; Jose, J.; Khadjavi, A.; Cavallo, F.; Quaglino, E.; Panariti, A.; Rivolta, I.; Benintende, E.; Varetto, G.; Argenziano, M.; Troia, A.; Cavalli, R.; Guiot, C. 2H,3H-Decafluoropentane-Based Nanodroplets: New Perspectives for Oxygen Delivery to Hypoxic Cutaneous Tissues. *PLoS One* **2015**, *10*, No. e0119769.

(6) Song, G.; Ji, C.; Liang, C.; Song, X.; Yi, X.; Dong, Z.; Yang, K.; Liu, Z. TaOx decorated perfluorocarbon nanodroplets as oxygen reservoirs to overcome tumor hypoxia and enhance cancer radiotherapy. *Biomaterials* **2017**, *112*, 257−263.

(7) Wang, W.; Cheng, Y.; Yu, P.; Wang, H.; Zhang, Y.; Xu, H.; Ye, Q.; Yuan, A.; Hu, Y.; Wu, J. Perfluorocarbon regulates the intratumoural environment to enhance hypoxia-based agent efficacy. *Nat. Commun.* **2019**, *10*, No. 1580.

(8) Castro, C. I.; Briceno, J. C. Perfluorocarbon-Based Oxygen Carriers: Review of Products and Trials. *Artif. Organs* **2010**, *34*, 622−634.

(9) Cabrales, P.; Friedman, J. M. HBOC Vasoactivity: Interplay Between Nitric Oxide Scavenging and Capacity to Generate Bioactive Nitric Oxide Species. *Antioxid. Redox Signaling* **2013**, *18*, 2284−2297.

(10) Bhandari, P.; Novikova, G.; Goergen, C. J.; Irudayaraj, J. Ultrasound beam steering of oxygen nanobubbles for enhanced bladder cancer therapy. *Sci. Rep.* **2018**, *8*, No. 3112.

(11) Bhandari, P.; Wang, X.; Irudayaraj, J. Oxygen Nanobubble Tracking by Light Scattering in Single Cells and Tissues. *ACS Nano* **2017**, *11*, 2682−2688.

(12) Bhandari, P. N.; Cui, Y.; Elzey, B. D.; Goergen, C. J.; Long, C. M.; Irudayaraj, J. Oxygen nanobubbles revert hypoxia by methylation programming. *Sci. Rep.* **2017**, *7*, No. 9268.

(13) Kheir, J. N.; Polizzotti, B. D.; Thomson, L. M.; O'Connell, D. W.; Black, K. J.; Lee, R. W.; Wilking, J. N.; Graham, A. C.; Bell, D. C.; McGowan, F. X. Bulk Manufacture of Concentrated Oxygen Gas-Filled Microparticles for Intravenous Oxygen Delivery. *Adv. Healthcare Mater.* **2013**, *2*, 1131−1141.

(14) Kwan, J. J.; Kaya, M.; Borden, M. A.; Dayton, P. A. Theranostic Oxygen Delivery Using Ultrasound and Microbubbles. *Theranostics* **2012**, *2*, 1174−1184.

(15) Swanson, E. J.; Mohan, V.; Kheir, J.; Borden, M. A. Phospholipid-Stabilized Microbubble Foam for Injectable Oxygen Delivery. *Langmuir* **2010**, *26*, 15726−15729.

(16) Seekell, R. P.; Lock, A. T.; Peng, Y.; Cole, A. R.; Perry, D. A.; Kheir, J. N.; Polizzotti, B. D. Oxygen delivery using engineered microparticles. *Proc. Natl. Acad. Sci. U.S.A.* **2016**, *113*, 12380−12385.

(17) Yang, C.; Xiao, H.; Sun, Y.; Zhu, L.; Gao, Y.; Kwok, S.; Wang, Z.; Tang, Y. Lipid Microbubbles as Ultrasound-Stimulated Oxygen Carriers for Controllable Oxygen Release for Tumor Reoxygenation. *Ultrasound Med. Biol.* **2018**, *44*, 416−425.

(18) McEwan, C.; Owen, J.; Stride, E.; Fowley, C.; Nesbitt, H.; Cochrane, D.; Coussios, C. C.; Borden, M.; Nomikou, N.; McHale, A. P.; Callan, J. F. Oxygen carrying microbubbles for enhanced sonodynamic therapy of hypoxic tumours. *J. Controlled Release* **2015**, *203*, 51−56.

(19) Culver, N. Dextran. In *Handbook of Pharmaceutical Excipients*; 8th ed.; American Pharmaceutical Association, Washington, DC, 2017; pp 298−302.

(20) Alam, Z.; Muyibi, S. A.; Toramae, J. Statistical optimization of adsorption processes for removal of 2,4-dichlorophenol by activated carbon derived from oil palm empty fruit bunches. *J. Environ. Sci.* **2007**, *19*, 674−677.

(21) Gu, B.; Linehan, B.; Tseng, Y.-C. Optimization of the Büchi B-90 spray drying process using central composite design for preparation of solid dispersions. *Int. J. Pharm.* **2015**, *491*, 208−217.

(22) Rahman, N.; Nasir, M. N-(((2-((2-Aminoethyl)amino)ethyl)-amino)methyl)-4-sulfamoylbenzamide Impregnated Hydrous Zirconium Oxide as a Novel Adsorbent for Removal of Ni(II) from Aqueous Solutions: Optimization of Variables Using Central Composite Design. *ACS Omega* **2019**, *4*, 2823−2832.

(23) Allison, S. D.; Manning, M. C.; Randolph, T. W.; Middleton, K.; Davis, A.; Carpenter, J. F. Optimization of Storage Stability of Lyophilized Actin Using Combinations of Disaccharides and Dextran. *J. Pharm. Sci.* **2000**, *89*, 199−214.

(24) Yasuda, K.; Matsushima, H.; Asakura, Y. Generation and reduction of bulk nanobubbles by ultrasonic irradiation. *Chem. Eng. Sci.* **2019**, *195*, 455−461.

(25) Schoonheydt, R. A.; Johnston, C. T. Chapter 5 - Surface and Interface Chemistry of Clay Minerals. In *Developments in Clay Science*; Bergaya, F.; Lagaly, G., Eds.; Elsevier, 2013; Vol. *5*, pp 139−172.

(26) Cavalli, R.; Bisazza, A.; Giustetto, P.; Civra, A.; Lembo, D.; Trotta, G.; Guiot, C.; Trotta, M. Preparation and characterization of dextran nanobubbles for oxygen delivery. *Int. J. Pharm.* **2009**, *381*, 160−165.

(27) Chen, X.; Wu, B.; Jayawardana, K. W.; Hao, N.; Jayawardena, H. S. N.; Langer, R.; Jaklenec, A.; Yan, M. Magnetic multivalent trehalose glycopolymer nanoparticles for the detection of mycobacteria. *Adv. Healthcare Mater.* **2016**, *5*, 2007−2012.

(28) Almalik, A.; Alradwan, I.; Kalam, M. A.; Alshamsan, A. Effect of cryoprotection on particle size stability and preservation of chitosan nanoparticles with and without hyaluronate or alginate coating. *Saudi Pharm. J.* **2017**, *25*, 861−867.

(29) Nirmalkar, N.; Pacek, A. W.; Barigou, M. On the Existence and Stability of Bulk Nanobubbles. *Langmuir* **2018**, *34*, 10964−10973.
(30) FDA*Pharmaceutical Microbiology Manual*; FDA, 2020; pp 1−92.
(31) Jin, F.; Li, J.; Ye, X.; Wu, C. Effects of pH and Ionic Strength on the Stability of Nanobubbles in Aqueous Solutions of α-Cyclodextrin. *J. Phys. Chem. B* **2007**, *111*, 11745−11749.
(32) Kundukad, B.; Udayakumar, G.; Grela, E.; Kaur, D.; Rice, S. A.; Kjelleberg, S.; Doyle, P. S. Weak acids as an alternative anti-microbial therapy. *Biofilm* **2020**, *2*, No. 100019.
(33) Song, R.; Peng, S.; Lin, Q.; Luo, M.; Chung, H. Y.; Zhang, Y.; Yao, S. pH-Responsive Oxygen Nanobubbles for Spontaneous Oxygen Delivery in Hypoxic Tumors. *Langmuir* **2019**, *35*, 10166−10172.
(34) Krupka, T. M.; Solorio, L.; Wilson, R. E.; Wu, H.; Azar, N.; Exner, A. A. Formulation and Characterization of Echogenic Lipid−Pluronic Nanobubbles. *Mol. Pharm.* **2010**, *7*, 49−59.
(35) FDA, SAS, FDA Drug Formulation Stability Program http://www.fda.gov/cder/sas/. 1992.
(36) Guideline, I. H. T. *Evaluation for Stability Data q1e*, International Conference on Harmonisation of Technical Requirements for Registration of Pharmaceuticals for Human Use, 2003; pp 1−19.
(37) Lee, H.-y.; Wu, P.-c.; Lee, Y.-j. stab: An R package for drug stability data analysis. *Comput. Methods Prog. Biomed.* **2010**, *100*, 140−148.
(38) Huang, S.-L.; McPherson, D. D.; MacDonald, R. C. A method to co-encapsulate gas and drugs in liposomes for ultrasound-controlled drug delivery. *Ultrasound Med. Biol.* **2008**, *34*, 1272−1280.
(39) Kim, Y. C.; Nishida, T. Nature of interaction of dextran sulfate with lecithin dispersions and lysolecithin micelles. *J. Biol. Chem.* **1977**, *252*, 1243−1249.
(40) Kokavec, J.; Min, S. H.; Tan, M. H.; Gilhotra, J. S.; Newland, H. S.; Durkin, S. R.; Grigg, J.; Casson, R. J. Biochemical analysis of the living human vitreous. *Clin. Exp. Ophthalmol.* **2016**, *44*, 597−609.
(41) REDDY, D. V. N.; KINSEY, V. E. Composition of the Vitreous Humor in Relation to That of Plasma and Aqueous Humors. *Arch. Ophthalmol.* **1960**, *63*, 715−720.
(42) Techologies, S. C. How to Create a Hypoxic Environment for Cell Culture . https://www.stemcell.com/how-to-create-a-hypoxic-environment-for-cell-culture.html (accessed Sept 11, 2020).
(43) Hartsock, M. J.; Cho, H.; Wu, L.; Chen, W.-J.; Gong, J.; Duh, E. J. A Mouse Model of Retinal Ischemia-Reperfusion Injury Through Elevation of Intraocular Pressure. *J. Visualized Exp.* **2016**, No. e54065.
(44) Masuzawa, K.; Jesmin, S.; Maeda, S.; Kaji, Y.; Oshika, T.; Zaedi, S.; Shimojo, N.; Yaji, N.; Miyauchi, T.; Goto, K. A model of retinal ischemia-reperfusion injury in rats by subconjunctival injection of endothelin-1. *Exp. Biol. Med.* **2006**, *231*, 1085−1089.
(45) Minhas, G.; Anhad, A. Animal Models of Retinal Ischemia. In *Brain Injury Pathogenesis, Monitoring, Recovery and Management*; IntechOpen, 2011; pp 153−174.
(46) Bui, B. V.; He, Z.; Vingrys, A. J.; Nguyen, C. T. O.; Wong, V. H. Y.; Fortune, B. Using the electroretinogram to understand how intraocular pressure elevation affects the rat retina. *J. Ophthalmol.* **2013**, *2013*, No. 262467.
(47) Cabrera, C. L.; Wagner, L. A.; Schork, M. A.; Bohr, D. F.; Cohan, B. E. Intraocular pressure measurement in the conscious rat. *Acta Ophthalmol. Scand.* **1999**, *77*, 33−36.
(48) Smedowski, A.; Pietrucha-Dutczak, M.; Kaarniranta, K.; Lewin-Kowalik, J. A rat experimental model of glaucoma incorporating rapid-onset elevation of intraocular pressure. *Sci. Rep.* **2014**, *4*, No. 5910.
(49) Eshaq, R. S.; Wright, W. S.; Harris, N. R. Oxygen delivery, consumption, and conversion to reactive oxygen species in experimental models of diabetic retinopathy. *Redox Biol.* **2014**, *2*, 661−666.
(50) Yu, D.-Y.; Cringle, S. J. Oxygen Distribution and Consumption within the Retina in Vascularised and Avascular Retinas and in Animal Models of Retinal Disease. *Prog. Retinal Eye Res.* **2001**, *20*, 175−208.
(51) Yu, D.-Y.; Cringle, S. J. Low oxygen consumption in the inner retina of the visual streak of the rabbit. *Am. J. Physiol.: Heart Circ. Physiol.* **2004**, *286*, H419−H423.
(52) Cugati, S.; Varma, D. D.; Chen, C. S.; Lee, A. W. Treatment Options for Central Retinal Artery Occlusion. *Curr. Treat. Options Neurol.* **2013**, *15*, 63−77.
(53) Medrano, C. J.; Fox, D. A. Oxygen consumption in the rat outer and inner retina: light- and pharmacologically-induced inhibition. *Exp. Eye Res.* **1995**, *61*, 273−84.
(54) Green, J. E. New tables for oxygen saturation in seawater. *J. Mar. Res.* **1967**, *24*, 140−147.
(55) Varma, D.; Lee, A. W.; Chen, C. S. Reply: 'A review of central retinal artery occlusion: clinical presentation and management'. *Eye* **2014**, *28*, 1270.
(56) Sampias, C.; Rolls, G. H&E staining overview: a guide to best practices . https://www.leicabiosystems.com/knowledge-pathway/he-staining-overview-a-guide-to-best-practices/ (accessed Aug 20, 2019).
(57) Wang, X.; Cui, Y.; Irudayaraj, J. Single-Cell Quantification of Cytosine Modifications by Hyperspectral Dark-Field Imaging. *ACS Nano* **2015**, *9*, 11924−11932.
(58) Giannelli, S. G.; Luoni, M.; Castoldi, V.; Massimino, L.; Cabassi, T.; Angeloni, D.; Demontis, G. C.; Leocani, L.; Andreazzoli, M.; Broccoli, V. Cas9/sgRNA selective targeting of the P23H Rhodopsin mutant allele for treating retinitis pigmentosa by intravitreal AAV9.PHP.B-based delivery. *Hum. Mol. Genet.* **2018**, *27*, 761−779.
(59) Marrocco, E.; Indrieri, A.; Esposito, F.; Tarallo, V.; Carboncino, A.; Alvino, F. G.; De Falco, S.; Franco, B.; De Risi, M.; De Leonibus, E. α-synuclein overexpression in the retina leads to vision impairment and degeneration of dopaminergic amacrine cells. *Sci. Rep.* **2020**, *10*, No. 9619.

https://doi.org/10.1021/acsanm.1c00084
ACS Appl. Nano Mater. XXXX, XXX, XXX−XXX